# Crystal dynamics of $\delta$ fcc Pu-Ga alloy by high-resolution inelastic x-ray scattering

Joe Wong,[1,*] M. Krisch,[2] D. L. Farber,[1] F. Occelli,[1] R. Xu,[3] T.-C. Chiang,[3] D. Clatterbuck,[1] A. J. Schwartz,[1] M. Wall,[1] and C. Boro[1]

[1]*Lawrence Livermore National Laboratory, University of California, P.O. Box 808, Livermore, California 94551, USA*

[2]*European Synchrotron Radiation Facility, BP 220, F-38043 Grenoble Cedex, France*

[3]*Department of Physics and Frederick Seitz Materials Research Laboratory, University of Illinois at Urbana-Champaign, 1110 West Green Street, Urbana, Illinois 61801, USA*

(Received 26 October 2004; revised manuscript received 24 March 2005; published 23 August 2005)

We have used a *microbeam on large grain sample* concept to carry out inelastic x-ray scattering experiments to measure the phonon dispersion curves of a fcc $\delta$-phase Pu-Ga alloy along the main symmetry directions of the cubic lattice. This approach obviates experimental difficulties with conventional inelastic neutron scattering due to the high absorption cross section of the common $^{239}$Pu isotope and the nonavailability of large (millimeter size) single crystal materials for Pu and its alloys. A classical Born-von Kármán force constant model was used to model the experimental results, and up to fourth nearest neighbor interactions had to be included to obtain sufficient agreement. Several unusual features including, a large elastic anisotropy, a small shear elastic modulus $(C_{11}-C_{12})/2$, a positive kink in the $T_1[0\xi\xi]$ branch, and a pronounced bending (toward lower energy) of the $T[\xi\xi\xi]$ branch near the $L$ point in the Brillouin zone are found. These features are discussed in light of the various phase transformations of $\delta$ plutonium. The phonon dispersion data also provide a critical test and benchmark for theoretical treatments of highly correlated $5f$ electron systems.

DOI: 10.1103/PhysRevB.72.064115 PACS number(s): 78.70.Ck, 61.50.Ks, 63.20.Dj, 64.70.Kb

## I. INTRODUCTION

Plutonium (Pu) is certainly the most astonishing member of the actinides, the class of the elements in which the $5f$ electron shell is progressively filled. Indeed, in the early part of this series (Th, Pa, U, and Np), the $5f$ electrons contribute to the bonding between atoms. The $5f$ participation in bonding results in an atomic volume dependence on electron population similar to that of the transition metal series. On the other hand, the heavier members of the actinide series (Am, Cm, and beyond) have larger atomic volumes that are almost independent of the $5f$ electron population. This behavior resembles those of the lanthanide elements; the $5f$ states are localized and do not participate in the bonding. In Pu, the $5f$ electrons are "on the edge,"[1] and it is this unique $5f$ configuration that gives this element a host of unusual properties.[2,3] Since the discovery of Pu in 1941, the element's eccentricities have both awed and perplexed researchers. Although the element's complexity and unpredictability have rendered it a challenge to study, scientists persist because of the need to understand and predict plutonium's behavior under various temperatures and pressures and to determine how the element's physical properties might vary over time. Understanding its properties is indeed critical for the safe handling, use, and long-term storage of this highly toxic and radioactive material.[4]

The most notably unusual property of Pu is perhaps the presence of five solid-state allotropic phase transformations in the pure element. The $\alpha$ phase, which is stable from low temperature to 122 °C, transforms successively to $\beta\rightarrow\gamma\rightarrow\delta\rightarrow\delta'\rightarrow\varepsilon\rightarrow$ liquid with increasing temperature[3] accompanied by large volume expansions and collapses along the way to the melt. The pure metal melts at a relatively low temperature ~640 °C to yield a liquid which is higher in density than that of the solid from which it melts. The fcc (face-centered-cubic) $\delta$ phase is the equilibrium phase in the range 319–451 °C, and has a density of 15.92 g/cc. This high temperature $\delta$ phase can be stabilized or more correctly retained at room temperature and below by alloying with small amounts of Group III metals such as Al or Ga.[5] In doing so, the metastable $\delta$-phase field is expanded from high temperature to room temperature and below. Moreover, alloys of $\delta$ Pu-Ga are known to transform directly to the $\alpha$ or $\alpha'$ monoclinic phase, bypassing both the $\gamma$ and $\beta$ phases via a martensiticlike transformation[3,5,6] which is displacive in nature and diffusionless. In many systems that undergo a martensitic phase transformation, such as NiTi, NiAl, and $Ni_2MnGa$, significant phonon softening is observed in the transverse acoustic mode.[7]

Phonon dispersion curves (PDC) are very fundamental to the derivation of material properties such as force constants, sound velocities, elastic, and thermodynamic properties, and to the study phase stability, electron-phonon coupling (charge-density waves), structural relaxation, etc. PDCs are key experimental data to the understanding of basic and often times intriguing properties of Pu materials, their phase changes, and associated phase stability. Yet, PDC measurements on Pu and its alloys with conventional inelastic neutron scattering (INS) are hindered by the facts that (i) Pu has a high neutron absorption cross section for the most common $^{239}$Pu isotope, and (ii) the large single crystals of Pu (a few millimeter cube) required for INS experiments are not available. These limitations have recently been overcome experimentally by the application of the high resolution inelastic x-ray scattering (HRIXS) technique, combined with a microbeam on large grain sample concept[8] by focusing a high brightness x-ray beam on large single-crystal domains in a polycrystalline specimen. Furthermore, only recently have theoretical computations of the Pu PDCs begun to overcome the difficulties in treating the $5f$ electrons accurately within

 

the standard first-principles methods.[9–12] Thus, until very recently, the PDCs for Pu-bearing systems have remained essentially unknown experimentally[8] and theoretically.[11]

The paper is organized as follows. Experimental details are presented in Sec. II, while the data and lattice dynamical calculations are presented in Sec. III. Section IV discusses the Born-von Kármán analysis, phonon-derived elastic and thermodynamic properties, phonon softening and phase trans-formations, an anomaly in the $T_1[\xi\xi 0]$ branch, and theoretical considerations. Our conclusions are summarized in Sec. V.

## II. EXPERIMENTAL DETAILS

Our samples were large-grain polycrystalline specimens prepared by a strain-enhanced re-crystallization technique[13] from an fcc $\delta$ Pu-Ga alloy containing 2 at. % Ga. A cylinder of the homogenized alloy, 2.8 mm diameter $\times$ 2 mm high was first uniaxially compressed by 6% and annealed at 460 °C in a vacuum ($5\times10^{-5}$ Torr) for five days. Two such strain-annealed cycles were employed. The doubly annealed cylinder was then sliced at 45 deg to the cylinder axis into three slices, each $\sim$500 $\mu$m thick using a low speed diamond (150 $\mu$m wide blade) saw. The discs were lapped with a succession of lapping films, 600 grit SiC, 30, 12, and 3 $\mu$m $\gamma$-$Al_2O_3$ to a thickness of $\sim$40 $\mu$m. A fine polish with 1 $\mu$m diamonds followed to remove $\sim$12 $\mu$m from each side, yielding a thickness of $\sim$16–18 $\mu$m. The samples were then electropolished from both sides using a TEM (transmission electron microscopy) electropolishing system such that a shallow dimple was electrochemically removed from both sides of the disc specimens to render a final thickness of $\sim$8–10 $\mu$m. This thickness is about one absorption length for $\delta$-Pu (Ref. 14) at 21.747 keV allowing for optimal IXS signals in transmission geometry. This procedure produced a microstructure with an average grain size of $\sim$90 $\mu$m as shown in Fig. 1. The samples were dip coated in liquid polyamide and cured at 50 °C for 1 h. This provided the first containment layer. The polyamide coated Pu-Ga foil was then loaded into a leak-proof stainless steel cell in a dry nitrogen atmosphere. The cell contained a pair of kapton windows each 125 $\mu$m thick which provide a second level of containment. An additional metal containment was used for each sample cell for shipment from Livermore, California to Grenoble, France.[15]

High resolution IXS experiments were conducted on beamline ID28 at the European Synchrotron Radiation Facility (ESRF) in Grenoble, France. The storage ring was operating at an electron energy of 6 GeV and injection current of 200 mA. The synchrotron radiation was monochromatized at 21.747 keV utilizing the Si(11 11 11) configuration to yield a total instrumental energy resolution of 1.8 meV full width at half maximum (FWHM) with the dimensions of the focused x-ray beam 30 $\mu$m horizontal $\times$ 60 $\mu$m vertical FWHM (see Fig. 1). With this beam, the flux on the sample was measured to be $\sim3\times10^9$ photons/s. The scattered photons were energy analyzed by five crystal analyzers in Rowland circle geometry employing the same reflection order as the high-resolution backscattering monochromator. The momentum

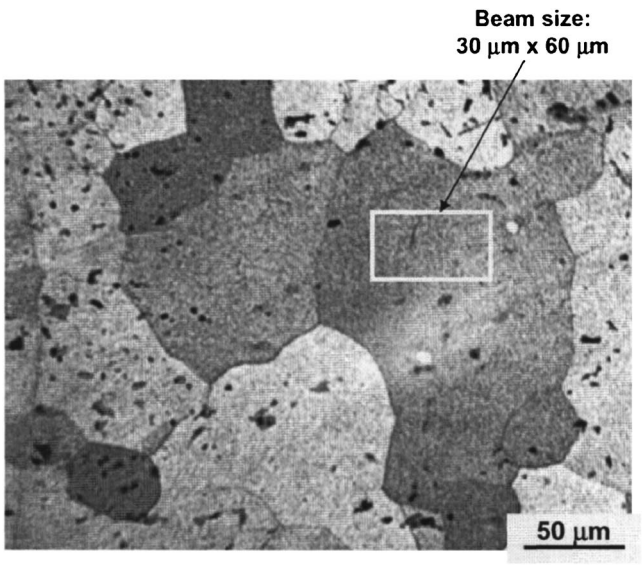


FIG. 1. Optical micrograph showing the large-grain microstructure of the fcc Pu-Ga 2 at. % alloy used in this study. The white box denotes the footprint on the sample of a 30 $\mu$m $\times$ 60 $\mu$m x-ray beam used to collect the HRIXS phonon spectra.

transfer, $Q=2k_0\sin(\theta_s/2)$, where $k_0$ is the wave vector of the incident photons and $\theta_s$ the scattering angle, was selected by rotating the spectrometer arm in the horizontal plane. The momentum resolution was set by slits to 0.4 $nm^{-1}$. An online fluorescent screen, coupled to a charge-coupled device (CCD) camera, allowed us to map and select single-crystal domains in the specimen, and orient them according to the requirements of the scattering geometry for the longitudinal and transverse acoustic phonon branches. With the small beam dimensions, single-crystal domains could be selected with a typical mosaic spread ranging between 0.5 and 1.5 deg. In the longitudinal geometry, after appropriate momentum transfer corrections,[16] the spectra of all five analyzers could be utilized. This was not possible for the transverse scans, and therefore the spectrum of only one analyzer was utilized. The energy scans were performed by varying the monochromator temperature while the analyzer temperature was kept constant. Conversion from the temperature scale to the energy scale was accomplished by using the following relation: $\Delta E/E=\alpha\Delta T$, where $\alpha=2.58\times10^{-6}$ $K^{-1}$ is the linear thermal expansion coefficient of Si at room temperature. Details of the HRIXS instrumentation have been described elsewhere.[17] All phonon spectra in this study were collected with the sample at room temperature.

## III. RESULTS

Typical IXS spectra (Fig. 2) are shown for longitudinal acoustic (LA) phonons along the [111] direction at selected reduced momentum transfer values ($\xi\xi\xi$). At a given $\boldsymbol{q}$ value, the count rate with error bars is plotted versus the energy of the analyzer. Each spectrum in Fig. 2 results from a sum of two individual 4-h scans. For each scan, the integration time per data point was 90 s. The spectra are each characterized by an elastic contribution centered at zero energy and two

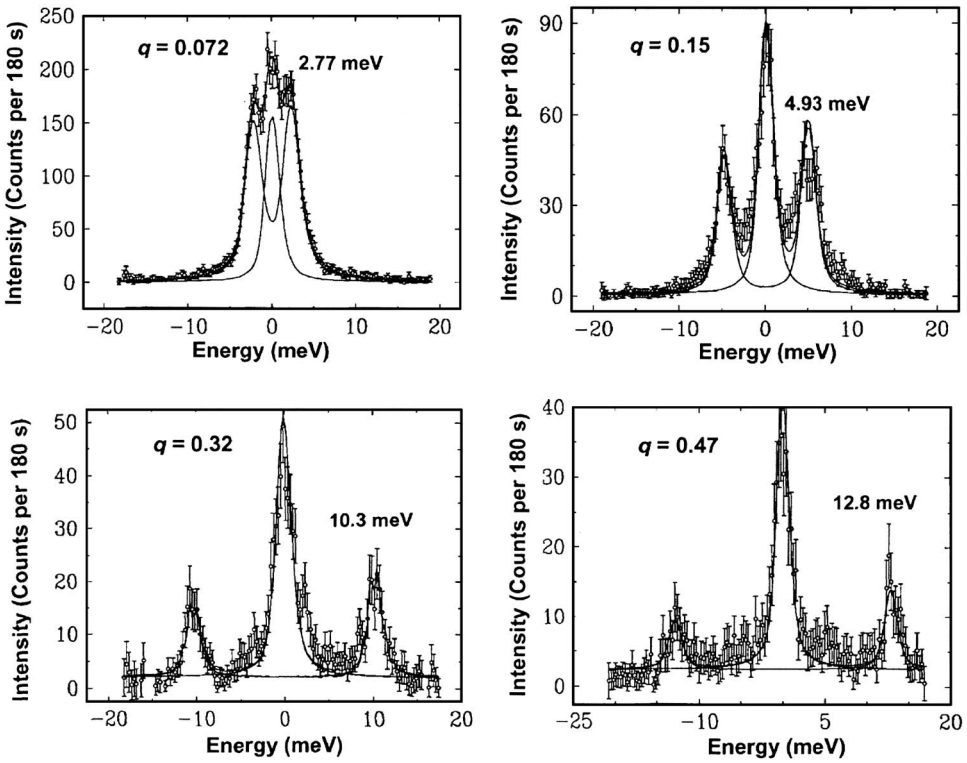


FIG. 2. Representative inelastic x-ray scattering spectra for the longitudinal acoustic phonon branch along the [111] direction in a $\delta$ Pu-2 at. % Ga alloy. The experimental data (points) are shown together with the results of the best fit model (lines) of the phonon and elastic contributions. In each panel, the reduced phonon wave vector $\xi$ is indicated to the left of the spectra and the phonon energy to the right.

inelastic contributions, corresponding to the creation (energy-loss, Stokes) and annihilation (energy gain, anti-Stokes) of an acoustic phonon. In order to extract the phonon energies, the spectra were fitted to a model function convoluted with the experimentally determined resolution function, by using a standard $\chi^2$ minimization procedure. This function consisted of a pair of Lorentzians for the Stokes and anti-Stokes excitations with their intensity ratio governed by the thermal phonon population factor, and a single Lorentzian for the central Rayleigh line.

Values of the phonon energies for the three main symmetry directions of the $\delta$ Pu-Ga fcc structure, with estimates of overall errors resulting from the $\chi^2$ minimization algorithm, are given in Table I. The experimental phonon dispersion curves along these symmetry directions are plotted as points in Fig. 3, together with a fit (solid lines) obtained by means of a standard Born-von Kármán (B-vK) force constant model.[18] An adequate fit to the experimental dispersions is obtained with this method if interactions up to the fourth nearest neighbor are included. Along the $[\xi 00]$ and $[\xi\xi\xi]$ directions, the transverse modes are degenerate and $\zeta$, the direction of vibration of the single atom in the unit cell, may lie in any direction normal to $\boldsymbol{q}$. Along the $[\xi\xi 0]$ direction, the two transverse modes are distinct with $\zeta$ lying in the $[01\bar{1}]$ and [001] directions for $T_1$ and $T_2$ respectively.

Three unusual features in the PDCs of $\delta$ Pu-Ga alloy are noteworthy: (a) similarity in the slopes of the LA($\xi$00) and TA($\xi$00) branches; (b) a kink in the $T_1(\xi\xi 0)$ branch suggestive of a Kohn anomaly,[19] and (c) a pronounced bending of the TA($\xi\xi\xi$) branch near the $L$ point. These features will be discussed in detail below.

## IV. DISCUSSION

### A. Born-von Kármán analysis

The experimental dispersion curves can be analyzed using the classical Born-von Kármán (B-vK) model with various coordination shells of interacting neighbors. Using a procedure of linear least squares fitting to the dispersions, interatomic force constants as well as interplanar force constants can be determined.[20] In a fcc lattice there is insufficient information in the dispersion curves along the principal symmetry directions to permit a fit beyond the fourth nearest neighbors (4NN). Constraints on the long-range force constants must be imposed to include higher neighbors. For example, two axially symmetric constraints are needed for a six nearest neighbor (6NN) model and four for an eight nearest neighbor (8NN) model (see Table II).

A series of B-vK calculations has been performed using models with 2NN to 8NN to fit the IXS data. The interatomic force constants obtained from these models are listed in Table II. As seen in Fig. 3 (solid lines), when no constraints are imposed and the forces extending to 4NN are considered, a reasonable fit to the dispersion curves is obtained. In Fig. 4, the goodness of fit, $\chi^2$, is plotted versus the number of neighbors included in the fit. At 3NN, $\chi^2$ drops significantly but decreases much more slowly upon including additional neighbors. In fact, beyond 4NN, the long-range force constants turn out to be much smaller. Extending the fit to eighth neighbors improves the goodness of the fit somewhat.

As noted by Dutton *et al.*,[21] in the fcc lattice, fourth neighbors are the most distant which can be reached in two *nearest-neighbor* steps. From this structural consideration it seems reasonable that the force constants for neighbors more

TABLE I. Normal mode phonon energies for the symmetry branches in a $\delta$ Pu-2 at. % Ga alloy at room temperature.

| $L(0,0,\xi)$ | | $T(0,0,\xi)$ | |
|---|---|---|---|
| $\xi$ | (meV) | $\xi$ | (meV) |
| 0 | 0 | 0 | 0 |
| 0.185 | 2.38±0.3 | 0.15 | 1.93±0.1 |
| 0.296 | 4.23±0.2 | 0.2 | 2.52±0.1 |
| 0.407 | 6.0±0.2 | 0.3 | 3.82±0.15 |
| 0.506 | 7.45±0.2 | 0.4 | 4.79±0.13 |
| 0.619 | 8.85±0.3 | 0.6 | 6.17±0.08 |
| 0.729 | 10.4±0.2 | 0.75 | 6.72±0.07 |
| 0.838 | 11.8±0.2 | 0.9 | 6.93±0.08 |
| 0.951 | 12.6±0.3 | 1 | 6.92±0.09 |
| 0.941 | 12.21±0.4 | | |
| **L(0,$\xi$,$\xi$)** | | **$T_2$(0,$\xi$,$\xi$)** | |
| **$\xi$** | **(meV)** | **$\xi$** | **(meV)** |
| 0 | 0 | 0 | 0 |
| 0.1 | 2.42±0.06 | 0.2 | 3.57±0.1 |
| 0.2 | 4.63±0.12 | 0.4 | 6.89±0.15 |
| 0.25 | 6.13±0.14 | 0.6 | 9.75±0.25 |
| 0.35 | 8.53±0.3 | 0.8 | 12.34±0.4 |
| 0.4 | 9.23±0.11 | | |
| 0.51 | 10.28±0.3 | **$T_1$(0,$\xi$,$\xi$)** | |
| 0.56 | 10.37±0.4 | **$\xi$** | **(meV)** |
| 0.66 | 10.65±0.2 | 0 | 0 |
| 0.72 | 9.72±0.4 | 0.2 | 1.45±0.05 |
| 0.81 | 8.54±0.4 | 0.3 | 2.14±0.06 |
| | | 0.45 | 3.56±0.1 |
| **L($\xi$,$\xi$,$\xi$)** | | 0.5 | 3.9±0.1 |
| **$\xi$** | **(meV)** | 0.6 | 5.01±0.15 |
| 0 | 0 | 0.7 | 5.43±0.3 |
| 0.072 | 2.27±0.1 | 0.85 | 6.49±0.3 |
| 0.1 | 3.11±0.12 | | |
| 0.15 | 4.93±0.28 | **T($\xi$,$\xi$,$\xi$)** | |
| 0.2 | 6.41±0.15 | **$\xi$** | **(meV)** |
| 0.23 | 7.45±0.15 | 0 | 0 |
| 0.28 | 9.02±0.3 | 0.075 | 1.22±0.1 |
| 0.32 | 10.27±0.2 | 0.1 | 1.52±0.07 |
| 0.35 | 10.9±0.2 | 0.15 | 2.164±0.06 |
| 0.4 | 11.91±0.3 | 0.2 | 2.56±0.06 |
| 0.43 | 12.1±0.4 | 0.3 | 2.83±0.06 |
| 0.45 | 12.6±0.3 | 0.4 | 2.34±0.06 |
| 0.47 | 12.8±0.3 | 0.5 | 1.98±0.0 |
| 0.48 | 12.8±0.3 | | |

distant than fourth have distinctly smaller values. Furthermore, it is interesting to note that the 4NN model for a fcc lattice includes a total of 54 atoms about a central atom: 12 *(110)* neighbors from the first coordination shell; 6 *(200)* neighbors from the second shell; 24 *(211)* neighbors from the third; and 12 *(220)* neighbors from the fourth shell. By composition, the 54 neighbors contain a Ga atom in the Pu-2 at. % Ga alloy, implying that the Ga has to be included in the crystal dynamics of the system within the B-vK framework.

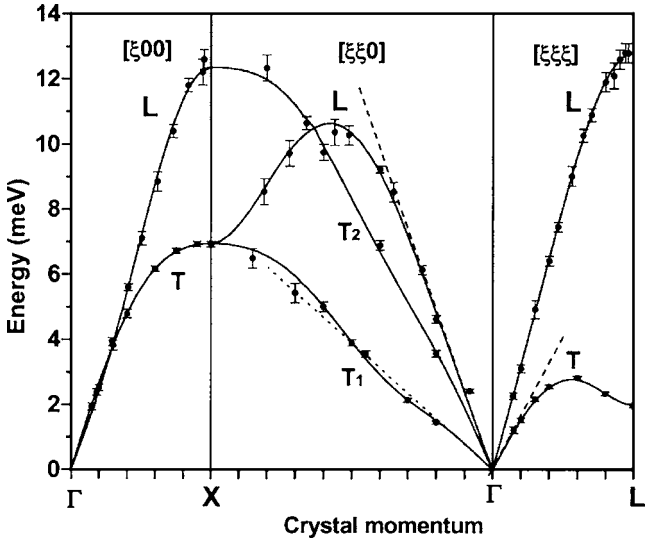


FIG. 3. Phonon dispersion curves of a $\delta$ fcc Pu-2 at. % Ga alloy at room temperature. The experimental points are plotted as circles, while the solid curves represent a fourth-nearest neighbor (4NN) Born-von Kármán model fit to the experimental data. The lattice parameter of the alloy is 0.4621 nm. Longitudinal and transverse modes are denoted $L$ and $T$, respectively The transverse branches along each of the $[\xi 00]$ and $[\xi\xi\xi]$ directions are degenerate. Along the $[\xi\xi 0]$ direction, the two transverse branches are distinct: $T_1[011]$ polarized along $\langle 01\bar{1}\rangle$ and $T_2[011]$ polarized along $\langle 001\rangle$. Note the pronounced bending of the $T[\xi\xi\xi]$ branch near the $L$ point.

### B. Elastic properties

The sound velocity $\nu$ associated with each of the phonon branches shown in Fig. 3 can be determined directly from a linear fit to the low q region around the $\Gamma$ point. These velocities are shown in Table III and are related to the elastic constants $C_{ij}$ by the Green-Christoffel equation.[22] For a cubic crystal, the elastic waves are purely longitudinal or purely transverse along the principal [100], [110], and [111] symmetry directions. The elastic constants for our Pu-Ga alloy given in Table III can be computed directly from the following simple relationships:[22]

$$\nu_L[100] = (C_{11}/\rho)^{1/2}, \quad \nu_T[100] = (C_{44}/\rho)^{1/2},$$

$$\nu_L[110] = ([C_{11} + C_{12} + 2C_{44}]/\rho)^{1/2},$$

$$\nu_{T1}[110] = ([C_{11} - C_{12}]/2\rho)^{1/2}, \quad \nu_{T2}[110] = (C_{44}/\rho)^{1/2},$$

$$\nu_L[111] = ([C_{11} + 2C_{12} + 4C_{44}]/3\rho)^{1/2},$$

$$\nu_T[111] = ([C_{11} - C_{12} + C_{44}]/3\rho)^{1/2} \qquad (1)$$

where $\rho$ is the mass density. For the Pu-2 at. % Ga alloy, $\rho$ equals 15.82 gm/cc at room temperature.

In a cubic crystal, if the interatomic forces are central (ie., purely radial, angle independent), then the Cauchy relation

TABLE II. Born-von Karman atomic force constants ($Nm^{-1}$).

| | 2NN | 3NN | 4NN | 5NN | 6NN | 7NN | 8NN |
|---|---|---|---|---|---|---|---|
| 1XX | 8.305 | 8.1149 | 9.4001 | 9.3616 | 9.2694 | 9.145 | 9.0172 |
| 1ZZ | −2.081 | −0.7228 | −2.1735 | −2.2841 | −2.3653 | −2.5584 | −2.1621 |
| 1XY | 8.557 | 11.3954 | 11.296 | 11.2949 | 11.2981 | 11.4838 | 11.5481 |
| 2XX | −1.929 | −0.7896 | −3.0938 | −2.9988 | −3.0892 | −2.9408 | −2.8591 |
| 2YY | −0.707 | −0.1357 | 0.9046 | 0.9719 | 1.1133 | 1.2634 | 0.6954 |
| 3XX | | −1.3769 | −0.5516 | −0.4387 | −0.3527 | −0.4641 | −0.7061 |
| 3YY | | 0.4561 | −0.2943 | −0.2915 | −0.2499 | −0.0928 | −0.1324 |
| 3YZ | | −0.587 | −0.4259 | −0.4245 | −0.4224 | −0.438 | −0.5226 |
| 3XZ | | −0.5389 | −0.3239 | −0.3074 | −0.3014 | −0.3401 | −0.2841 |
| 4XX | | | −0.0657 | −0.0284 | −0.0586 | −0.1854 | −0.0202 |
| 4ZZ | | | 0.9747 | 0.974 | 0.9729 | 1.0115 | 0.7709 |
| 4XY | | | −0.4969 | −0.538 | −0.5856 | −0.6857 | −0.8681 |
| 5XX | | | | −0.084 | −0.0582 | 0.0141 | 0.3726 |
| 5YY | | | | −0.0369 | −0.0141 | −0.1258 | 0.0303 |
| 5ZZ | | | | −0.0015 | −0.0694 | −0.1433 | −0.0125 |
| 5XY | | | | −0.0176 | −0.0165 | 0.0525 | 0.1284 |
| 6XX | | | | | −0.0698 | −0.1863 | −0.031 |
| 6YZ | | | | | 0.0255 | 0.0966 | 0.218 |
| 7XX | | | | | | 0.0003 | 0.0425 |
| 7YY | | | | | | 0.1319 | −0.0184 |
| 7ZZ | | | | | | −0.048 | −0.0279 |
| 7YZ | | | | | | −0.0056 | −0.0186 |
| 7XZ | | | | | | −0.0084 | −0.0279 |
| 7XY | | | | | | −0.0168 | −0.0557 |
| 8XX | | | | | | | −0.9241 |
| 8YY | | | | | | | 0.0101 |
| $\chi^2$ | 2010.8 | 67.8 | 35.6 | 33.7 | 27.7 | 21.1 | 14.1 |

Constraints for 8NN and 7NN: 8(5ZZ)=9(5YY)−5XX; 8(5XY)=3(5XX−5YY); 3(7YZ)=7XY; 2(7XZ)=7XY

Constraints for 6NN and 5NN: 8(5XY)=3(5XX−5YY)

No constraints for 4NN, 3NN and 2NN.

for the second order elastic constants is fulfilled.[23]

$$C_{44} = C_{12}. \tag{2}$$

Deviations from this relation account for the existence of noncentral forces. In Table IV, the experimental elastic constants of all fcc metals reported in the literature[24–44] are listed. Most of these elastic moduli were determined from inelastic neutron scattering, except for those of Ir,[25] Pt,[26] Rh,[27] and Th,[36] which were determined from ultrasonic measurements. The elastic constants for Pt were measured at 90 K,[26] and those of $\beta$-La (Ref 29) and $\gamma$-Fe (Ref 43) at 660 and 1428 K, respectively, at which the fcc phases of these two metals are thermodynamically stable. Deviations from the Cauchy relation, as defined by $C_{44}-C_{12}$ are also reported in Table IV. Th appears to be the only fcc metal that obeys the Cauchy equality with $C_{44}$–$C_{12}$ (within 0.2%), implying that the interatomic forces in Th are largely central. The rest of the fcc metals exhibit substantial deviation from Cauchy equality, implying that noncentral and angular forces are op-

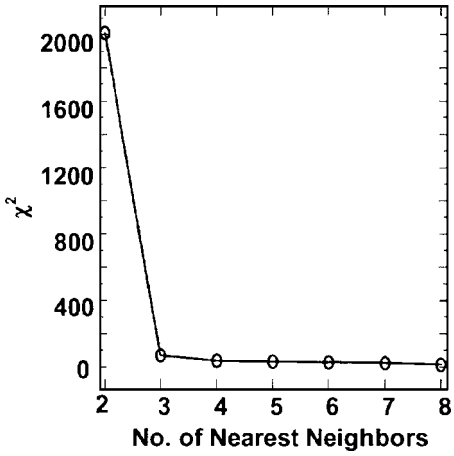


FIG. 4. A statistical estimate of the goodness of fit $\chi^2$ for a Born-von Kármán model plotted as a function of the number of nearest neighbors included in the model.

TABLE III. Sound velocities $\nu(\mathrm{ms}^{-1})$, and elastic moduli $C_{ij}$ for $\delta$ Pu-2 at. % Ga (GPa). The elastic moduli for both a Pu-3.4 at. % Ga alloy by ultrasonics and pure $\delta$ Pu calculated using DMFT are also listed for comparison.

| $\nu_L[100]=1586\pm20$ | | $\nu_L[110]=1894\pm20$ | | $\nu_L[111]=2080\pm30$ |
|---|---|---|---|---|
| $\nu_T[100]=1379\pm30$ | | $\nu_{T1}[110]=566\pm4$ | | $\nu_L[111]=979\pm45$ |
| | | $\nu_{T2}[110]=1411\pm16$ | | |
| System | $C_{11}$ | $C_{12}$ | $C_{44}$ | Remarks |
| $\delta$ Pu-2 at. % Ga | 35.3±1.4 | 25.5±1.5 | 30.53±1.1 | This work |
| $\delta$ Pu-3.4 at. % Ga | 36.28 | 26.73 | 33.59 | Ultrasonics[44] |
| $\delta$ Pu | 34.56 | 26.81 | 33.03 | DMFT[11] |

erative in the lattices. Furthermore, the deviation for most fcc metals is negative, i.e., $C_{44}<C_{12}$, whereas for Ir, $\gamma$-Ce, Yb, and $\delta$Pu-Ga, the deviation is positive, i.e., $C_{44}>C_{12}$. In the latter three systems, for which the phonon dispersions are known,[30,42] an unusual feature of their dispersion curves is that the $T$ and $L$ branches along $[\xi 00]$ have nearly the same velocity [see Figs. 3 and 7(a) for $\gamma$-Ce]. This implies an unusually high $T$-mode sound velocity (and thus a relatively high $C_{44}$ and a positive $C_{44}$–$C_{12}$). In the case of $\delta$Pu-Ga, it is useful to compare $[\xi\xi 0]T_1$ with $[\xi 00]T$ (Table V). One sees comparable first interplanar force constants. The second interplanar force constants are also similar but with opposite signs. For $[\xi 00]T$, both the first and second terms are positive, resulting in a reenforcement, making the system more rigid against transverse displacement. However, the signs are opposite for $[\xi\xi 0]T_1$. This results in a partial cancelation of the restoring forces, making the lattice softer for the corresponding mode. Thus, $[\xi 00]T$ has a larger slope than $[\xi\xi 0]T_1$ resulting in $C_{44}>C_{12}$.

Table IV reports also the anisotropy factor, defined[45] as the ratio of $C_{44}/C'$, where $C'=1/2[C_{11}-C_{12}]$, associated with the two nondegenerate transverse $T_2[\xi\xi 0]$ and $T_1[\xi\xi 0]$ branches [Eqs. (1)] in the phonon dispersion curves shown in Fig. 3. In fcc metals, the elastic anisotropy factor increases from simple $p$ metals like Al to transition metals and rare-earth metals up to a value of ~4. For the fcc Pu–2 at. % Ga alloy, our phonon data shows a high value of 6. By definition, the large anisotropy factor is directly related to the low speed of sound of $T_1[\xi\xi 0]$, since $2C_{44}/(C_{11}-C_{12})$ is proportional to the ratio of the speed of sound of the two transverse

TABLE IV. Elastic constants $C_{ij}$ of fcc metals (in units of GPa) at 300 K—Cauchy inequality: $C_{44}$–$C_{12}$, and anisotropy factor: $C_{44}/1/2[C_{11}$-$C_{12}]$. Except for Rh, Ir, Pt, Th, and Pu-Ga, all elastic moduli were determined from inelastic neutron scattering measurements.

| Metal | $C_{11}$ | $C_{12}$ | $C_{44}$ | Cauchy inequality $C_{44}$-$C_{12}$ | Anisotropy factor $2C_{44}/[C_{11}$-$C_{12}]$ | Reference |
|---|---|---|---|---|---|---|
| Al | 106.8 | 60.7 | 28.2 | −32.5 | 1.223 | 24 |
| Ir (ultrasonic) | 600 | 260 | 270 | +10 | 1.588 | 25 |
| Pt (90 K) (ultrasonic) | 346.7 | 250.7 | 76.5 | −174.2 | 1.594 | 26 |
| Rh (ultrasonic) | 413 | 194 | 184 | −10 | 1.680 | 27 |
| Ni | 250.8 | 150.0 | 123.5 | −26.5 | 2.450 | 28 |
| $\beta$-La (300 K) | 34.47 | 20.38 | 17.96 | −2.42 | 2.549 | 29 |
| $\gamma$-Ce | 24.1 | 10.2 | 19.4 | +9.2 | 2.79 | 30 |
| Pd | 227.1 | 176.1 | 71.7 | −104.4 | 2.811 | 31 |
| Au | 192.3 | 163.1 | 42.0 | −121.1 | 2.876 | 32 |
| Ag | 124.0 | 93.7 | 46.1 | −47.6 | 3.042 | 33 |
| Cu | 168.4 | 121.4 | 75.4 | −46.0 | 3.208 | 34 |
| Ca | 27.8 | 18.2 | 16.3 | −1.9 | 3.396 | 35 |
| Th (ultrasonic) | 75.3 | 48.9 | 47.8 | −0.11 | 3.621 | 36 and 37 |
| Sr | 15.3 | 10.3 | 9.9 | −0.4 | 3.960 | 38 |
| Pb | 49.5 | 42.3 | 14.9 | −27.4 | 4.138 | 39 and 40 |
| $\beta$-La (660 K) | *28.46* | *20.41* | *16.53* | *−3.88* | *4.106* | 41 |
| Yb | 18.6 | 10.3 | 17.7 | +7.4 | 4.265 | 42 |
| $\gamma$-Fe (1428 K) | 154 | 122 | 77 | −45 | 4.813 | 43 |
| $\delta$ Pu-Ga (IXS) [2 at. % Ga] | 35.30 | 25.5 | 30.53 | +5.03 | 6.059 | This work |
| $\delta$ Pu-Ga (ultra) [3.4 at. % Ga] | 36.28 | 26.73 | 33.59 | +6.86 | 7.03 | 44 |

TABLE V. Interplanar force constants ($Nm^{-1}$) for $\delta$ Pu-2 at. % Ga calculated from the 4NN B-vK model.

| Branch | $\Phi_1$ | $\Phi_2$ | $\Phi_3$ | $\Phi_4$ |
|---|---|---|---|---|
| $[00\xi]L$ | 70.552 | −11.138 | | |
| $[00\xi]T$ | 22.156 | 3.09 | | |
| $[0\xi\xi]L$ | 28.136 | 37.802 | −5.98 | −1.128 |
| $[0\xi\xi]T_2$ | 72.912 | −3.468 | −2.36 | 1.952 |
| $[0\xi\xi]T_1$ | 22.95 | −4.014 | −0.796 | 0.864 |
| $[\xi\xi\xi]L$ | 74.774 | −6.884 | | |
| $[\xi\xi\xi]T$ | 1.826 | 2.548 | | |

$[\xi\xi 0]$ phonon branches. This in turn is consistent with the respective values of the interplanar force constants, which are linear combinations of atomic force constants. As seen in Table V the first interplanar force constants $\Phi_1$ for the $T_2$ and $T_1[\xi\xi 0]$ branches are very different, the former being more than three times larger than the latter. [This is the main source of the anisotropy.]

The present result confirms an earlier ultrasonic measurement on a higher Ga (3.4 at. %) alloy by Ledbetter and Moment[44] who reported an anisotropy factor of 7 and discussed the elastic properties of $\delta$ Pu-Ga alloys in detail. The extremely high elastic anisotropy with regard to propagation of elastic waves in fcc Pu is also substantiated by a recent dynamical mean field theory (DMFT) calculation[11] which yielded an even higher theoretical anisotropy factor of 8 for pure $\delta$-Pu. More recent DFT (density functional theory) calculations[46] using various formalisms to describe several assumed magnetic configurations of $\delta$-Pu (disordered, ferromagnetic, nonmagnetic) yields anisotropy factor values ranging from 1.6 to 10, and not a single set of elastic constants from a given formalism agrees with those experimentally determined in this study to within a factor of two.

### C. Phonon density of states, lattice heat capacity and Debye temperature

Using the phonon dispersion relations derived from the 4NN Born-von Kármán model shown in Fig. 3, the phonon density of states (DOS) has been computed. The computation was carried out using a grid of $(2\pi/a)/500$, and the result is normalized such that the area under the curve corresponds to three states per atom. A Gaussian smoothing by 0.03 meV was applied to produce the final plot shown in Fig. 5(a). The peak at 11.7 meV in the DOS contains major contributions from all three $L$ branches and the $T_2(011)$ branch near the $X$ point. The peak at 6.2 meV has contributions from all branches except the $T(111)$ branch which contributes most significantly to the "rounded-off" feature at 2.1 meV. Critical points obtained from the symmetry points in the zone are indicated in the DOS plot.

The DOS has been used to compute the lattice specific heat $C_v$ as a function of temperature, and the result is presented in Fig. 5(b). At high temperature, $C_v$ approaches the classical Dulong and Petit limit of $3R = 5.96$ cal. $mole^{-1}$ $K^{-1}$, where $R$ is the molar gas constant. At

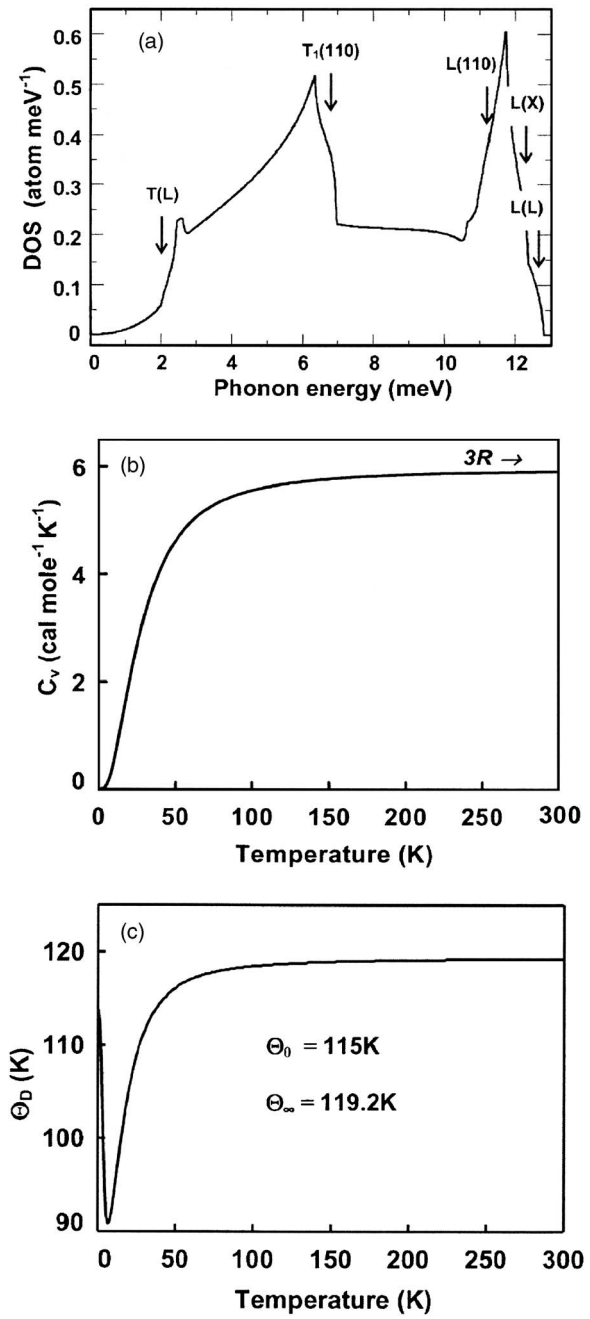


FIG. 5. (a) Density of states (DOS), (b) lattice specific heat, and (c) Debye temperature of a fcc Pu-2 at. % Ga alloy calculated from a 4NN Born-von Kármán model. Critical points in the DOS obtained from the symmetry points in the zone are indicated in (a).

low temperature, the electronic contribution $\gamma T$ to the total heat capacity becomes significant.[47,48] Indeed, by measuring the total heat capacities of a $\delta$-$Pu_{0.95}$ $Al_{0.05}$ alloy and pure $\alpha$-Pu at low temperatures down to 2 K and subtracting the lattice contribution derived from inelastic neutron scattering data,[49] Lashley *et al.*[50] found that the $\gamma$ value for the $\delta$ Pu-Al alloy is almost a factor of 4 higher than that for pure $\alpha$-Pu, suggesting proximity of the $\delta$ phase to a quantum critical point.

From the computed lattice specific heat, the Debye temperature $\Theta_D$ has also been computed as a function of tem-

TABLE VI. Calculated Debye temperatures $\Theta_D$ of fcc metals from DOS derived from B-vK modeling of experimental phonon dispersions.

| Metal | $\Theta_0$(K) | $\Theta_\infty$(K) | $\Theta_0 > \Theta_\infty$[a] | B-vK Model[b] | Reference |
|---|---|---|---|---|---|
| Ni | 450 | 385 | Y | 5NN | 28 |
| Al | 410 | 395 | Y | 8NN | 24 |
| Cu | 333 | 313 | Y | 6NN | 34 |
| $\gamma$-Fe | 324 | 330 | N | 6NN | 43 |
| Ag | 223 | 215 | Y | 4NN | 33 |
| Ca | 216 | 213 | Y | 8NN | 35 |
| Pd | [c] | 275 | | | 31 |
| Pt (90 K) | [c] | 230 | | | 26 |
| Au | 159 | 183 | N | 4NN | 32 |
| Th | 158 | 142 | Y | 7NN | 36 |
| $\beta$-La (300 K) | 139 | 122 | Y | 8NN | 29 |
| $\gamma$-Ce | 135 | 119 | Y | 8NN | 30 |
| $\beta$-La (660 K) | 134 | 123 | Y | 8NN | 41 |
| Yb | 109 | 105 | Y | 2NN | 42 |
| Pb | [c] | 88 | | >8NN | 39 |
| $\delta$ Pu-Ga (2 at. %) | 114 | 119 | N | 4NN | This work |
| $\delta$ Pu-Ga (1.9 at. %) | 120[d] | [c] | | EXAFS | 51 |
| $\delta$ Pu-Ga (3.4 at. %) | 115 | [c] | | Ultrasonics | 44 |
| $\delta$ Pu-Ga (6.8 at. %) | 127 | [c] | | Ultrasonics | 44 |
| $\delta$ Pu-Ga (10.2 at. %) | 133 | [c] | | Ultrasonics | 44 |

[a] $\theta_0$, $\theta_\infty$=Debye temperatures at 0 K and $\infty$ K, respectively. For all fcc metals listed above, $\theta_0 > \theta_\infty$, except for $\gamma$-Fe, Au, $\delta$ Pu-Ga.

[b] NN=nearest neighbors. 8NN means that interactions up to eight nearest neighbor have been taken into account for a good fit of the PDC data with the B-vK model.

[c] Not calculated.

[d] Derived from the Pu-Pu bond correlation. The corresponding Debye temperature from the Ga-Pu correlation is 188 K.

perature. This is plotted in Fig. 5(c). Above 100 K, the Debye temperature $\Theta_{D(\infty)}$ remains remarkably constant at a value of ~119 K. At 0 K, the calculated value $\Theta_{D(0)}$ is 114 K, which is in excellent agreement with the values of 115 and 120 K determined, respectively, from ultrasonic measurements[44] on a $\delta$ Pu-3.4 at. % Ga alloy and from extended x-ray-absorption fine structure (EXAFS) measurements[51] on a $\delta$ Pu-1.9 at. % Ga alloy. In Table VI the Debye temperatures of fcc metals calculated from phonon DOS derived from Born-von Kármán modeling of experimentally determined phonon dispersions are tabulated. It is interesting to note that Au, $\gamma$-Fe, and $\delta$ Pu-Ga are the only fcc metals with $\Theta_{D(0)} < \Theta_{D(\infty)}$. At low temperatures, only the low frequency modes are thermally occupied. A low Debye temperature implies a low average speed of sound. Thus, the average speed of sound in Pu-Ga is lower than what one might expect based on the high-temperature limit of the Debye temperature. The "positive dispersion" in the $T_1[\xi\xi 0]$ branch (discussed later in Sec. V) might be responsible for the low Debye temperature at $T=0$. Since at low temperatures, only the phonons around the $\Gamma$ point contribute, a lower Debye temperature means a lower average speed of sound near the $\Gamma$ point, which fits the behavior of the $T_1[\xi\xi 0]$ branch well. This branch has the lowest speed of sound (i.e., the lowest phonon energy near $\Gamma$) hence, the largest phonon population, and thus may be the major cause of the unusual trend in the Debye temperature. Similarly, Au (Ref. 32) and $\gamma$-Fe (Ref. 43) have a positive dispersion in the $T_1[\xi\xi 0]$ branch and both metals also have lower Debye temperatures at $T=0$.

It should be noted that the above discussion on Debye temperature is based on the dispersion curves measured at room temperature. As the temperature changes, the dispersion curves will likely change, and in fact, at ~170 K the fcc Pu-Ga alloy undergoes a phase transition to a monoclinic $\alpha$ phase[5] (see Sec. IV below). Thus, the Debye temperature at $T=0$ as seen in Fig. 5(c) is not the same Debye temperature *measured* at $T=0$.

### D. T($\xi\xi\xi$) branch bending and the $\delta \rightarrow \alpha'$ transformation

The experimental PDCs shown in Fig. 3 display a pronounced bending toward lower energies of the T$[\xi\xi\xi]$ branch near the $L$ point. A similar feature (but occurring at about twice the energy and at a higher crystal momentum toward the $L$ point) is also seen in a recent dynamic mean field theory (DMFT) calculation of the PDCs of $\delta$-Pu,[11] (Fig. 6). The bending of this T$[\xi\xi\xi]$ mode is rather unusual in fcc

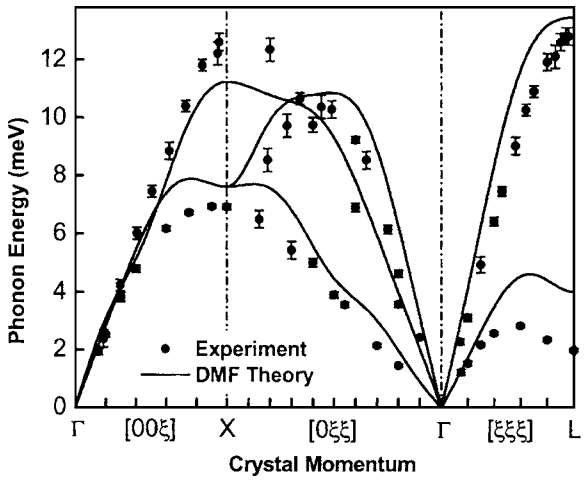


FIG. 6. Comparison of calculated phonon dispersions (lines) for pure $\delta$Pu using DMFT-linear response theory by Dai *et al.* (Ref 11) with the present experimental dispersions (circles) for a fcc $\delta$ Pu-Ga alloy, showing overall qualitative agreement.

metals, occurring in only two other systems: $\gamma$-Ce (Ref. 30) and $\beta$-La,[29,41] whose PDCs determined by inelastic neutron scattering are reproduced in Fig. 7. Temperature-dependent studies have shown that the $T[\xi\xi\xi]$ modes in these two rare-earth systems soften near the $L$ point at low temperature. Based on this evidence, it has been proposed that the observed phonon softening is related to the fcc $\rightarrow$double hexagonal close packed (dhcp) phase transformation which occurs in Ce and La at 283 and 660 K respectively.[30] By analogy, the observed bending of the $T[\xi\xi\xi]$ branch in the present experiment on the Pu-Ga alloy may be related to the $\delta \rightarrow \alpha'$ transformation which occurs upon cooling these materials to subambient temperatures.[5,52] Measurements of the temperature dependence of the PDCs are currently underway to validate this hypothesis.

The softening of the $T[\xi\xi\xi]$ branch is also consistent with the crystallography of transformations that occur in $\gamma$-Ce, $\beta$-La, and $\delta$ Pu-Ga alloys. In all cases, the parent phase is the fcc crystal structure which is composed of hexagonal-close-packed atomic planes stacked along the [111] direction with an *ABCABC*,…, stacking arrangement. The soft transverse mode at $L$ suggests that a (111) plane could be easily sheared relative to its neighboring atomic planes to form new stacking arrangements. In the case of Ce and La the product phase has a dhcp structure with an *ABACABAC*,…, stacking arrangement, while in the case of Pu-Ga alloys the product phase is a complex monoclinic structure[53] which can also be viewed as a distorted hexagonal close packed structure with an *ABABAB*,…, stacking arrangement. It is also possible that the phonon softening is related to the $\delta \rightarrow \gamma$ transformation which occurs in pure Pu and produces a phase with a face-centered orthorhombic structure[54] which can also be viewed as a stack of slightly distorted hexagonal packed atomic layers which have an *ABABAB*,…, stacking arrangement. The low energy of the necessary shearing processes involved in these transformations can be seen in the first interplanar force constant of the $T[\xi\xi\xi]$ mode (as derived from the 4NN B-vK model) which is more than an order of magnitude

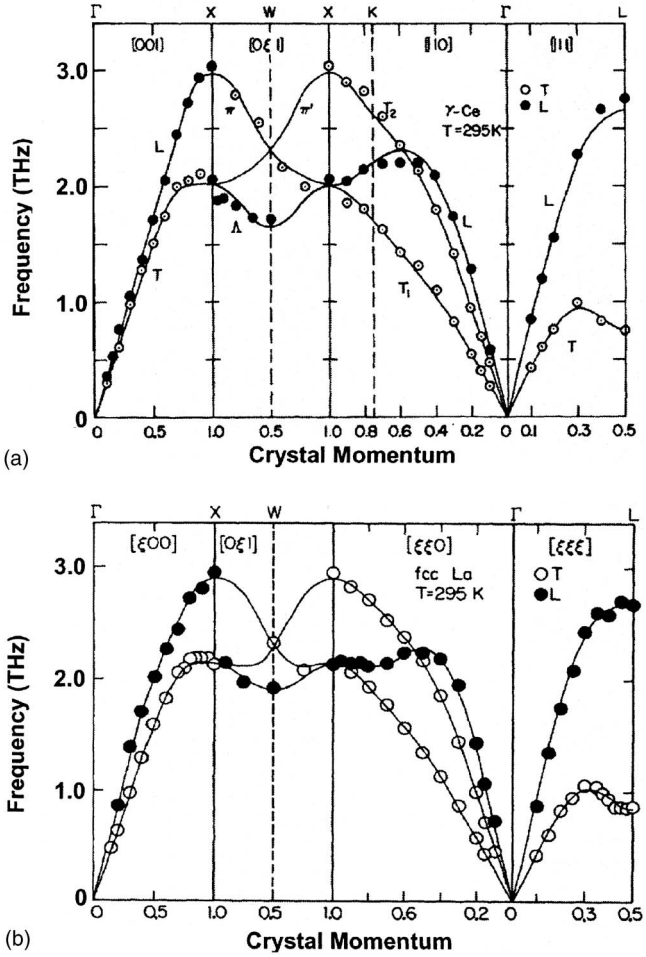


FIG. 7. Room temperature phonon dispersion curves of (a) fcc $\gamma$-Ce (Ref 30) and (b) fcc $\beta$-La,[29] showing bending of the $T[\xi\xi\xi]$ branch near the $L$ point similar to that observed in the current Pu-Ga alloy. In each case, the smooth curves represent a 8NN Born-von Kármán force-constant model fit to the inelastic neutron scattering data. (Reproduced with permission from the authors.)

smaller than those of the transverse modes in the other two directions (see Table V).

In order to more precisely relate the bending of the $T[\xi\xi\xi]$ branch to the $\delta \rightarrow \alpha'$ transformation in Pu-Ga alloys, we can employ the crystallographic models that have been developed by Adler *et al.*,[55] and more recently by Jin *et al.*[56] These models use as a starting point the crystallographic correspondence $(111)_\delta \| (020)_\alpha$ and $[-110]_\delta \| [100]_\alpha$ which has been established using transmission electron microscopy by Zocco *et al.*[57] Both sets of models predict stable transformation twins with $(205)_\alpha$ twin planes also in agreement with the TEM observations. The distortion required to transform a region of the fcc $\delta$ phase crystal structure to the monoclinic $\alpha'$ phase crystal structure can be decomposed into three elementary distortions.

(1) A shuffling operation transforms the fcc structure into a hcp structure by changing the stacking sequence of {111} planes.

(2) A homogeneous elastic strain distorts the hcp structure such that an enlarged 16 atom unit cell has *lattice* vec-

tors which match the *lattice* vectors of the $\alpha'$ phase.

(3) A set of periodic displacements modify the *basis* vectors of the distorted, enlarged hcp unit cell such that the $\alpha'$ crystal structure is formed. In this step the *lattice* vectors do not change, only the internal coordinates of the atoms with respect to these vectors. Thus this step does not produce any elastic strain.

The observed low phonon energy in $\delta$Pu-Ga near the $L$ point can be related to the shuffling operation described above. The shuffling operation requires that alternating (111) planes in the fcc lattice be rigidly translated in order to produce the hcp lattice. There are an infinite number of ways in which a shuffling can transform the fcc lattice into the hcp lattice. The simplest mode is a single elementary shuffle and is used in the correspondence suggested Adler *et al.*[55] which agrees with the TEM observations.[57] In this case, every other (111) layer is rigidly shifted by $1/6[-211]$. This shuffling operation is a combination of a zone boundary $T[\xi\xi\xi]$ phonon and a homogeneous shear parallel to the (111) plane. Thus, the experimentally observed bending of the $T[\xi\xi\xi]$ branch is consistent with the proposed model, but we should emphasize that it is only one component of the shuffle operation which itself is only one part of the entire transformation process.

Other more complex shuffling modes are also considered by Jin *et al.*[56] They all involve rigidly shifting {111} planes to modify the stacking sequence. In these cases, the shuffle includes one or more transverse phonons propagating in the $\langle 111\rangle$ direction but with different wave vectors. Again, a homogeneous shear parallel to the {111} plane is necessary to complete the shuffle in addition to the appropriate phonon. Each of these proposed shuffle modes lead to different predictions for the habit plane and volume fraction of each twin variant. Further experimental data is needed to clarify which shuffle mode is involved in the phase transformation. In all cases however, the low energy of the $T[\xi\xi\xi]$ branch near the $L$ point is consistent with the crystallographic models of the $\delta \rightarrow \alpha'$ transformation.

### E. Anomaly in the $T_1(\xi\xi 0)$ branch

In Fig. 3 the $T_1$ branch along $[\xi\xi 0]$ exhibits a "kink" with positive dispersion toward the $X$ point, similar to those observed in other fcc metals such as Th,[36] Au,[32] Pt,[26] and Pd.[31] The existence of the kink in the $T_1[\xi\xi 0]$ dispersion can graphically be shown from the dispersion data shown in Fig. 3. If one draws a straight line from the $\Gamma$ point through the one or two nearest data points to make an extension of the linear range of the dispersion curve, then the rest of the data points along the branch should usually distribute below this line for a normal branch (dash lines). However, this is not the case for the $T_1[\xi\xi 0]$ branch (dotted line), which shows clearly that the slope undergoes a positive upturn (kink) as we move away from the $\Gamma$ point. Moreover, the fitting results from the 4NN (solid lines in Fig. 3) to 8NN B-vK models all show an "upturn" in the $T_1[\xi\xi 0]$ branch. This kink also appears in the DMFT results of Dai *et al.*[11] shown in Fig. 6.

By analogy with other phonon anomalies observed in metals, the observed upturn in the $T_1[\xi\xi 0]$ branch is likely to be caused by electronic effects.[19] As the speed of sound of this mode is given by $\sqrt{C'/\rho}$, ($\rho$=density), it is clear that this anomaly is directly responsible for the small value of $C'$ and implies a soft response of the system to a volume-conserving tetragonal distortion. This anomaly has been associated[8] with the phase transformations of Pu at high temperature from $\delta \rightarrow \delta'$ (body centered tetragonal) $\rightarrow \varepsilon$ (body centered cubic). These transformations could involve just a tetragonal distortion of this type via the so-called Bain path.[58]

### F. Theoretical considerations

As evident in Fig. 6, the present x-ray results validate the main qualitative predictions of a recent DMFT dispersion calculation by Dai *et al.*[11] for $\delta$-Pu in terms of (i) a large bending toward the lower energy of the $T[\xi\xi\xi]$ branch near $L$, (ii) a kink in the $T_1[0\xi\xi]$ branch, and (iii) a low shear elastic modulus $C'$. Such experimental-theoretical agreements lend credence to the DMFT approach for theoretical treatments of correlated $5f$ electron systems as exemplified by $\delta$-Pu. Quantitatively however, differences exist. These are the position of the energy maximum along the $T[\xi\xi\xi]$ branch, the position of the Kohn-like kink along the $T_1[0\xi\xi]$ branch, and the bending of the calculated $T[\xi 00]$ branch near the $X$ point, which is not observed experimentally in the fcc Pu-Ga alloy.

Dai *et al.*[11] also calculated the phonon dispersion curves for the bcc $\varepsilon$-Pu phase with the DMFT method and found that several modes are totally unstable at $T=0$. Existence (stability) of $\varepsilon$-Pu at high temperature[3] was attributed to anharmonicity and final temperature phonon entropy.[11] On the other hand, the calculated phonon dispersion curves for $\delta$-Pu shown in Fig. 6 were also computed at $T=0$. All modes are found to be stable (no negative frequencies) at all $\mathbf{q}$ values, in spite of the fact that pure $\delta$-Pu is the equilibrium phase only at high temperature in the range 592–724 K.[3]

More recently, using a simple inclusion of electron correlations in a Friedel model of the density of $f$-electron states, and an empty-core pseudopotential treatment for the three free electrons per atom, Harrison[59] calculated the phonon dispersion curves of $\delta$-Pu, which contain neither the kink in the $T_1[\xi\xi 0]$ branch nor any bending in the $T(\xi\xi\xi)$ branch observed experimentally in this study. The derived elastic constants were also in poor agreement with both the earlier ultrasonic work[44] and our IXS data. The predicted anisotropy factor was 19 compared with an experimental factor of 6–7 (Table IV). These differences between the experimental and calculated phonon dispersions are significant and thus provide the framework for refined theoretical treatments[12] and further experiments in Pu and other $5f$ systems.

## V. CONCLUDING REMARKS

In this paper we have rendered a crystal dynamics analysis of the phonon dispersion curves (PDCs) of a fcc $\delta$ Pu-Ga alloy determined recently[8] using a *microbeam on a large grain sample* experimental concept with high resolution inelastic x-ray scattering to obviate the roadblocks of phonon dispersion measurements on Pu-bearing materials with con-

ventional inelastic neutron scattering. Our PDC data confirms directly the very high elastic anisotropy of fcc Pu-Ga alloys (highest of all known fcc metals), discovered almost three decades ago from very careful ultrasonic measurements.[44] More important is the pronounced bending observed for the $T[\xi\xi\xi]$ branch near the $L$ point. The low energy of this branch is found to be crystallographically consistent with the meta-stability of the fcc phase of the Pu-Ga alloy and its transformation to a pseudohexagonal closed pack, monoclinic $\alpha'$ phase via a martensitic transformation. A temperature dependence study of the $T[\xi\xi\xi]$ branch, which is now underway, will hopefully clarify the role of lattice dynamics in the $\delta \rightarrow \alpha'$ transformation in Pu-Ga alloys. This study provides a needed bonafide data set for realistic calculations and simulations of thermodynamic and other physical properties for Pu and its alloys. The phonon dispersion results also provide a critical test for theoretical treatments of highly correlated $5f$ electron systems, as exemplified by recent dynamical-mean-field-theory calculations for $\delta$ plutonium[11] with excellent qualitative and semiquantitative agreement between theory and experimental data.

## ACKNOWLEDGMENTS

This work was performed under the auspices of the U. S. Department of Energy by the University of California, Lawrence Livermore National Laboratory under Contract No. W-7405-Eng-48 and the U.S. Department of Energy by the University of Illinois Frederick Seitz Materials Research Laboratory under Grant No. DEFG02-91ER45439. We are thankful to Francesco Sette for his support and encouragement in this project, and to P. Berkvens and P. Colomp for their advice and technical assistance.

*Electronic address: wong10@llnl.gov

[1] G. Lander, Science **301**, 1057 (2003).
[2] A. M. Boring and J. L. Smith, Los Alamos Sci. **26**, 91 (2000).
[3] S. S. Hecker, Los Alamos Sci. **26**, 290 (2000).
[4] R. Jeanloz, Phys. Today **12**, 44 (2000).
[5] S. S. Hecker, Prog. Mater. Sci. **49**, 429 (2004).
[6] J. T. Orme, M. E. Faiers, B. J. Ward, in *Proceedings of 5th Conference in Plutonium Another Actinides*, edited by by H. Blank and R. Lindner (North Holland Publishing, New York, 1976), p. 761.
[7] A. Zheludev S. M. Shapiro, P. Wochner, A. Schwartz, M. Wall, and L. E. Tanner, Phys. Rev. B **51**, 11310 (1995).
[8] Joe Wong, M. Krisch, D. Farber, F. Occelli, A. Schwartz, Tai-C. Chiang, M. Wall, C. Boro, and R. Xu, Science **301**, 1078 (2003).
[9] M. E. Manley, G. H. Lander, H. Sinn, A. Alatas, W. L. Hults, R. J. McQueeney, J. L. Smith, and J. Willit, Phys. Rev. B **67**, 052302 (2003).
[10] S. Y. Savrasov, G. Kotliar, and E. Abrahams, Nature (London) **410**, 793 (2001).
[11] X. Dai, S. Y. Savrasov, G. Kotliar, A. Migliori, H. Ledletter, and E. Abrahams, Science **300**, 953 (2003).
[12] G. Kotliar and D. Vollhardt, Phys. Today **57**, 53 (2004).
[13] J. C. Lashley, M. G. Stout, R. A. Pereyra, M. S. Blau, and J. D. Embury, Scr. Mater. **44**, 2815 (2001).
[14] W. H. McMaster, N. Nerr del Grande, J. H. Mallett, and J. H. Hubbel, Lawrence Radiation Laboratory Report No. UCRL-50/74 sec. 2 Rev., 1969 (unpublished).
[15] ESRF Procedures for experiments using radioactive samples on beam lines other than BM20.
[16] F. Occelli, M. Krisch, P. Loubeyre, F Sette, R. Le Toullec, C. Masciovecchio, and J.-P Rueff, Phys. Rev. B **63**, 224306 (2001).
[17] M. D'Astuto, P. K. Mang, P. Giura, A. Shukla, P. Ghigna, A. Mirone, M. Braden, M. Greven, M. Krisch, and F. Sette, Phys. Rev. Lett. **88**, 167002 (2002); H. Requardt, J. E. Lorenzo, P. Monceau, R. Currat, M. Krisch, Phys. Rev. B **66**, 214303 (2002).
[18] M. Born and K. Huang, *Dynamical Theory of Crystal Lattices* (Clarendon Press, Oxford, England, 1954).
[19] W. Kohn, Phys. Rev. Lett. **2**, 393 (1959).
[20] E. C. Svensson, B. N. Brockhouse, and J. W. Rowe, Phys. Rev. **155**, 619 (1967).
[21] D. H. Dutton, B. N. Brockhouse, and A. P. Miiller, Can. J. Phys. **50**, 2915 (1972).
[22] G. P. Srivastava, *The Physics of Phonons* (Adam Hilger, Bristol, England, 1990).
[23] Reference 18, p. 142.
[24] C. Kittel, *Introduction to Solid State Physics*, 3rd ed. (Wiley, New York, 1967), p. 122.
[25] R. E. MacFarlane, J. A. Rayne, and C. K. Jones, Phys. Lett. **20**, 234 (1966).
[26] R. E. MacFarlane, Phys. Lett. **18**, 91 (1965).
[27] E. Walker, J. Ashkenazi, and M. Dacorogna, Phys. Rev. B **24**, 2254 (1981).
[28] R. J. Birgeneau, J. Cordes, G. Dolling, and A. D. B. Woods, Phys. Rev. **136**, A1359 (1964).
[29] C. Stassis, G. S. Smith, B. N. Harmon, K.-M. Ho, and Y. Chen, Phys. Rev. B **31**, 6298 (1985).
[30] C. Stassis, T. Gould, O. D. McMasters, K. A. Gschneidner Jr., and R. M. Nicklow, Phys. Rev. B **19**, 5746 (1979); C. Stassis, C.-K. Loong, O. D. McMasters, and R. M. Nicklow, *ibid.* **25**, 6485 (1982).
[31] J. A. Rayne, Phys. Rev. **118**, 1545 (1960).
[32] J. W. Lynn, H. G. Smith, and R. M. Nicklow, Phys. Rev. B **8**, 3493 (1973).
[33] W. Drexel, Z. Phys. **205**, 281 (1972).
[34] W. C. Overton, Jr. and J. Gaffney, Phys. Rev. **98**, 969 (1955).
[35] C. Stassis, J. Zaretsky, D. K. Misemer, H. L. Skriver, B. N. Harmon, and R. M. Nicklow, Phys. Rev. B **27**, 3303 (1983).
[36] P. E. Armstrong, O. N. Carlason, and J. F. Smith, J. Appl. Phys. **30**, 36 (1959).
[37] R. A. Reese, S. K. Sinha, and D. T. Peterson, Phys. Rev. B **8**, 1332 (1973).
[38] U. Buchenau, M. Heiroth, H. R. Schober, J. Evers, and G. Oehlinger, Phys. Rev. B **30**, 3502 (1984).

[39] D. L. Waldorf, Bull. Am. Phys. Soc. **5**, 170 (1960).
[40] B. N. Brockhouse, T. Arase, G. Caglioti, K. Rao, and A. D. Woods, Phys. Rev. **128**, 1099 (1962).
[41] C. Stassis, C.-K. Loong, and J. Zarestky, Phys. Rev. B **26**, 5426 (1982).
[42] C. Stassis, C.-K. Loong, C. Theisen, and R. M. Nicklow, Phys. Rev. B **26**, 4106 (1982)
[43] J. Zarestky and C. Stassis, Phys. Rev. B **35**, 4500 (1987).
[44] H. M. Ledbetter and R. L. Moment, Acta Metall. **24**, 891 (1976).
[45] C. Zener, *Elasticity and Anelasticity of Metal* (University Chicago Press, Chicago, IL, 1948), p. 16
[46] P. Soderlind, A. Landa, B. Sadigh, L. Vitos, and A. Ruban, Phys. Rev. B **70**, 144103 (2004).
[47] A. P. Miiller and B. N. Brockhouse, Can. J. Phys. **49**, 704 (1971).
[48] A. P. Miiller and B. N. Brockhouse, Phys. Rev. Lett. **20**, 798 (1968).
[49] R. J. McQueeney, A. C. Lawson, A. Migliori, T. M. Kelley, B. Fultz, M. Ramos, B. Martinez, J. C. Lashley, and Sven C. Vogel, Phys. Rev. Lett. **92**, 146401 (2004).
[50] J. C. Lashley, J. Singleton, A. Migliori, J. B. Betts, R. A. Fisher, J. L. Smith, and R. J. McQueeney, Phys. Rev. Lett. **91**, 205901 (2003).
[51] E. J. Nelson, K. J. M. Blobaum, M. A. Wall, P. G. Allen, A. J. Schwartz, and C. H. Booth, Phys. Rev. B **67**, 224206 (2003).
[52] S. S. Hecker and L. F. Timofeeva, Los Alamos Sci. **26**, 244 (2000).
[53] W. H. Zachariasen and F. H. Ellinger, Acta Crystallogr. **16**, 777 (1963).
[54] W. H. Zachariasen and F. H. Ellinger, Acta Crystallogr. **8**, 431 (1955).
[55] P. H. Alder, G. B. Olson, and D. S. Margolies, Acta Metall. **34**, 2053 (1986).
[56] Y. M. Jin, Y. U. Wang, A. G. Khachaturyan, C. R. Krenn, and A. J. Schwartz (unpublished).
[57] T. G. Zocco, M. F. Stevens, P. H. Alder, R. T. Sheldon, and G. B. Olson, Acta Metall. Mater. **38**, 2275 (1990).
[58] R. W. K. Honeycombe, *Steels: Microstructure and Properties* (Edward Arnold Publ., London, 1980), p. 81.
[59] W. A. Harrison, Phys. Rev. B **69**, 113106 (2004).